Title

Estimating fetal dose from tube current-modulated (TCM) and fixed tube current (FTC) abdominal/pelvis CT examinations

Journal

Medical Physics, 46(6)

ISSN

0094-2405

Authors

Hardy, Anthony J
Angel, Erin
Bostani, Maryam
et al.

Publication Date

2019-06-01

DOI

10.1002/mp.13499

Peer reviewed

Measure and Evaluate MRgRT **3D Distortion**

distortion check

CLOUD SOFTWARE FOR EVALUATION OF IMAGE DISTORTION

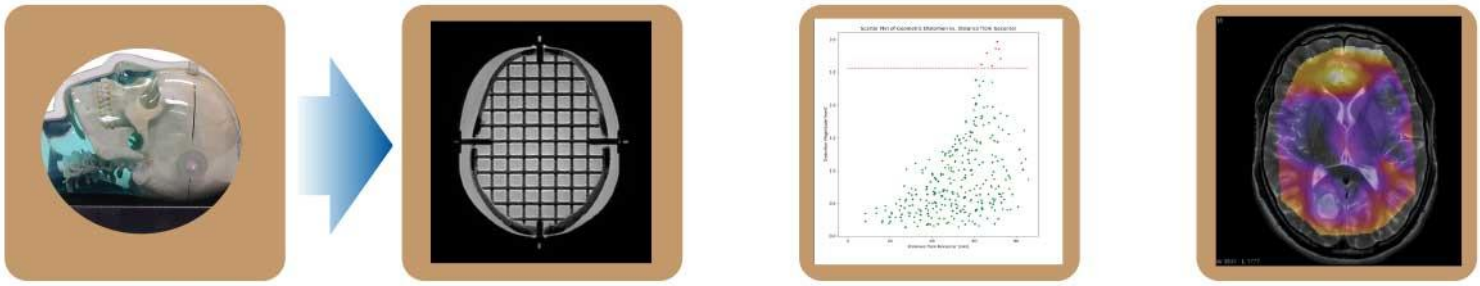

SCAN | **UPLOAD IMAGES** | **REVIEW REPORTS & TREND ANALYSIS** | **EXPORT DICOM OVERLAYS TO TPS**

- CIRS proprietary materials simulate distortion due to susceptibility & chemical shifts typical to clinical patient scans

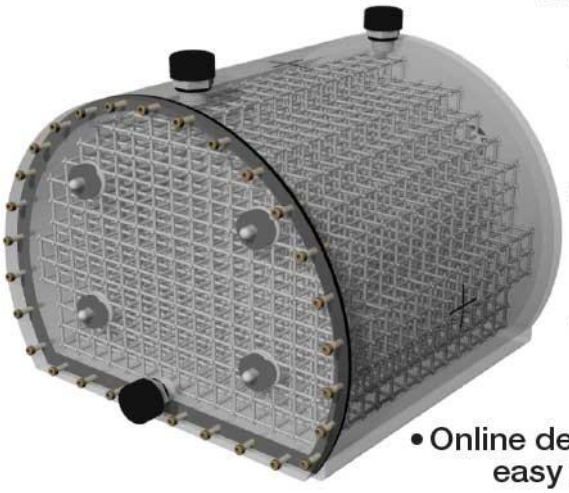

- Density of physical control points optimized to bring interpolation close to linearity
- Cloud based solution frees user of operating system and hardware constraints
- Quickly & automatically analyze complete MR data sets
- Online deployment facilitates collaboration, easy review and portability of results

Large Field Grid Phantom
2623 Physical Control Points

Visit us at ECR, Booth 128!

Inter-cranial Grid Phantom
335 Physical Control Points

CIRS

900 Asbury Ave. • Norfolk, Virginia 23513 • USA • Tel: 757-855-2765 • **WWW.CIRSINC.COM**

Estimating Fetal Dose from Tube Current Modulated (TCM) and Fixed Tube Current (FTC) Abdominal/Pelvis CT Examinations

Anthony J. Hardy, MS[1,2]; Erin Angel, PhD[3]; Maryam Bostani, PhD[1,2]; Chris Cagnon, PhD[1,2]; and Michael McNitt-Gray, PhD[1,2]

[1]Department of Radiology, David Geffen School of Medicine, University of California, Los Angeles, Los Angeles, California, 90024

[2]Physics and Biology in Medicine Graduate Program, David Geffen School of Medicine, University of California, Los Angeles, Los Angeles, California, 90024

[3]Canon Medical Systems USA, Inc., Tustin, CA, 92780

***Corresponding Author**

924 Westwood Blvd, Suite 650

Los Angeles, CA 90024, USA

Phone: (310) 481-7558

ahardy@mednet.ucla.edu

ABSTRACT

Purpose

The purpose of this work was to estimate scanner independent $CTDI_{vol}$-to-fetal-dose coefficients for tube current modulated (TCM) and fixed tube current (FTC) CT examinations of pregnant patients of various gestational ages undergoing abdominal/pelvic CT examinations.

This article has been accepted for publication and undergone full peer review but has not been through the copyediting, typesetting, pagination and proofreading process, which may lead to differences between this version and the Version of Record. Please cite this article as doi: 10.1002/mp.13499

Methods

For 24 pregnant patients of gestational age from less than 5 to 36 weeks who underwent clinically-indicated CT examinations, voxelized models of maternal and fetal (or embryo) anatomy were created from abdominal/pelvic image data. Absolute fetal dose (D_{fetus}) was estimated using Monte Carlo (MC) simulations of helical scans covering the abdomen and pelvis for TCM and FTC scans. Estimated TCM schemes were generated for each patient model using a validated method that accounts for patient attenuation and scanner output limits for one scanner model and were incorporated into MC simulations. FTC scans were also simulated for each patient model with multidetector row CT scanners from four manufacturers. Normalized fetal dose estimates, nD_{fetus}, was obtained by dividing D_{fetus} from the MC simulations by $CTDI_{vol}$. Patient size was described using water equivalent diameter (D_w) measured at the three-dimensional geometric centroid of the fetus. Fetal depth (DE_f) was measured from the anterior skin surface to the anterior part of the fetus. nD_{fetus} and D_w were correlated using an exponential model to develop equations for fetal dose conversion coefficients for TCM and FTC abdominal/pelvic CT examinations. Additionally, bivariate linear regression was performed to analyze the correlation of nD_{fetus} with D_w and fetal depth (DE_f). For one scanner model, nD_{fetus} from TCM were compared to FTC and the SSDE conversion coefficients (*f*-factors) from AAPM Report 204. nD_{fetus} from FTC simulations was averaged across all scanners for each patient ($\overline{nD_{fetus}}$). $\overline{nD_{fetus}}$ was then compared with SSDE *f*-factors and correlated with D_w using an exponential model and with D_w and DE_f using a bivariate linear model.

Results

For TCM, the coefficient of determination (R^2) of nD_{fetus} and D_w was observed to be 0.73 using an exponential model. Using the bivariate linear model with D_w and DE_f, an R^2 of 0.78 was observed. For the TCM technology modeled, TCM yielded nD_{fetus} values that were on average 6% and 17% higher relative to FTC and SSDE *f*-factors, respectively. For FTC, the R^2 of $\overline{nD_{fetus}}$ with respect to D_w was observed to be 0.64 using an exponential model. Using the bivariate linear model, an R^2 of 0.75 was

observed for $\overline{nD_{fetus}}$ with respect to D_w and DE_f. A mean difference of 0.4% was observed between $\overline{nD_{fetus}}$ and SSDE *f*-factors.

Conclusion

Good correlations were observed for nD_{fetus} from TCM and FTC scans using either an exponential model with D_w or a bivariate linear model with both D_w and DE_f. These results indicate that fetal dose from abdomen/pelvis CT examinations of pregnant patients of various gestational ages may be reasonably estimated with models that include (1) scanner-reported $CTDI_{vol}$ and (2) D_w as a patient size metric, in addition to (3) DE_f if available. These results also suggest that SSDE *f*-factors may provide a reasonable (within ± 25%) estimate of nD_{fetus} for TCM and FTC abdomen/pelvis CT exams.

Keywords: Computed tomography, tube current modulation, Monte Carlo simulations, fetal dose, conceptus dose, embryo dose, radiation dose

I. INTRODUCTION

Performing CT exams on pregnant patients is occasionally necessary. In such cases, physicians, medical physicists, and/or radiation safety officers may need to estimate the radiation dose received by the conceptus (fetus or embryo) with a reasonable degree of accuracy due to the risks associated with irradiating developing radiosensitive organs such as red bone marrow.[1–3] Initial attempts to estimate the radiation dose a fetus would receive from a CT exam were based either on phantom measurements, Monte Carlo (MC) simulations of geometric phantoms, or a combination of the two.[4–13] The approach described by Felmlee et al., for example, uses anthropomorphic phantom measurements and measured CTDI values.[4] Some important limitations of these early efforts relate to

their use of simplified, geometric models and assumptions of non-varying maternal anatomy in a single-size patient model.

More recent methods for estimating radiation conceptus dose from CT exams of pregnant patients are typically based on MC simulations of pregnant patient anatomy representing a range of gestational ages and patient sizes.[14–20] However, many of these studies were limited in that they were either not based on actual pregnant patient anatomy, applied only to a single scanner model, or did not include a range of gestational ages. In addition, most of these methods have thus far been limited to fixed tube current (FTC) CT exams of pregnant patients. For example, the study conducted by Angel et al. examined the effects that maternal and fetal characteristics such as maternal size, gestational age, and fetal presentation have on fetal dose using MC simulations.[14] This work was based on voxelized patient models generated from a set of pregnant patients who underwent clinically indicated abdominal and pelvic CT examinations.[14] While the results of Angel et al. addressed the limitations of earlier studies by providing size-specific fetal dose estimates based on actual patient anatomy across a range of gestational ages, dose estimates were nevertheless limited to FTC CT exams of pregnant patients for a specific scanner model.

In the current context of CT dosimetry, nearly all CT exams are performed with attenuation-based tube current modulation (TCM). Additionally, Turner et al. developed scanner-independent, size-adjusted estimates of organ dose by normalizing organ doses from MC simulations of voxelized models by $CTDI_{vol}$.[21,22] The work of Turner et al. was incorporated into Size-Specific Dose Estimate (SSDE) in AAPM Report 204 and was subsequently extended in AAPM report 220 which described the attenuation-based size metric water equivalent diameter (D_w), which is defined as "x-ray attenuation of a patient in terms of a water cylinder having the same x-ray absorption."[23,24] The normalization metric of $CTDI_{vol}$ and the attenuation-based size metric of D_w are routinely used for generating predictive estimates of normalized organ dose. However, estimates reported by Angel et al. were based on a per 100 mAs normalization and patient size characteristics were described in terms of maternal perimeter.

Gu et al. conducted a study to estimate the effects of TCM on fetal doses for three computational phantoms representing pregnant patients of the gestational ages of 3, 6, and 9 months.[18,19] Since no TCM data existed for these computational phantoms, TCM schemes were instead selected from actual pregnant patients of gestational ages of 15, 20, and 31 weeks, and were appropriately applied to the computational phantoms. These selected TCM schemes were longitudinal modulation (z axis) only and did not include angular (x-y axis) modulation. This approach of necessity assumed that the TCM scheme for one patient matched the anatomy of another patient. This is crucial since TCM adjusts the tube current with respect to the attenuation characteristics of the patient in question. Additionally, as shown in Angel et al., fetal dose correlates strongly with a measure of maternal patient size but does not correlate with gestational age.[14]

Physical phantom studies have also been used to estimate fetal dose from CT with TCM at several gestational stages using anthropomorphic phantoms and MOSFETs.[13,20] While these studies do consider TCM, there is an inherent issue with estimating dose using small detectors. Even when considering a FTC study, the dose distribution within a patient is substantially non-uniform.[25] When this effect is combined with the non-uniform exposure patterns of TCM during a helical acquisition, the point detector is sampling only a certain location in a complex dose distribution environment. MC simulations can be used to estimate average fetal dose in a way that overcomes the limitations of measuring at single points inside a non-uniform dose distribution.

However, performing MC simulation for every pregnant patient undergoing CT examinations is a time prohibitive option. Therefore, the primary purpose of this investigation was to develop a patient size-specific method for estimating radiation dose to the embryo or fetus for pregnant patients undergoing abdominal/pelvic CT exams that accounts for the use of either TCM or FTC scanning techniques and applies to patients of different sizes and gestational ages. This investigation was meant to serve as an update to the study conducted by Angel et al. and used the same patient models. However, though the patient models used in this study were the same as those used by the study conducted by Angel et al., this study differs from the previous study in four distinct ways. (1) The study conducted by Angel et al. normalized fetal doses on a per 100 mAs basis whereas this study

used $CTDI_{vol}$ as normalization metric.[14] The normalization using $CTDI_{vol}$ employed in this study is consistent with AAPM Report 204.[23] For TCM scans, fetal doses were normalized by $CTDI_{vol}$ based on the average tube current across the entire scan. For FTC scans, the dose to the fetus was normalized by $CTDI_{vol}$ for each patient. (2) This study used D_w as metric of patient size from AAPM Report 220[24] while the study conducted by Angel et al.[14] used patient perimeter as the metric of patient size. (3) Multiple scanner models were included in the FTC simulations for this study to accommodate for the effects of scanner design. (4) The effects of TCM were included in this study whereas the Angel et al. study was limited to FTC. The results of this study were a set of scan technique-independent, $CTDI_{vol}$-to-fetal-dose coefficients for abdominal/pelvic CT, which can be applied to (a) either TCM or FTC scans, (b) patients of different sizes in terms of D_w, and (c) patients at various gestational stages of pregnancy. Additionally, as with Angel et al., this study also investigated using fetal depth (DE_f) in conjunction D_w for estimating $CTDI_{vol}$-to-fetal-dose coefficients.[14] Lastly, the resulting fetal dose coefficients were compared to SSDE conversion coefficients (*f*-factors) from AAPM Report 204 to investigate the use of SSDE as an estimate of fetal dose for either TCM or FTC scans. The SSDE *f*-factors are the conversion coefficients for adjusting the scanner-reported $CTDI_{vol}$ to account for patient size. AAPM Report 204 notes "that the actual dose to any given patient may differ from the value calculated using this report by 10% to 20%.[24]" Though not originally intended to be a measure of fetal dose, it is expected that the SSDE *f*-factors will become widely available. In addition to estimating fetal dose, this study therefore also sought to compare fetal dose from TCM and FTC to SSDE in order ascertain whether or not SSDE could be used as a surrogate for fetal dose.

II. MATERIALS AND METHODS

II.A. Voxelized patient cohort

The patient image data used in this investigation was previously collected by Angel et al. and is comprised of 24 pregnant patients of gestational ages ranging from less than 5 to 36 weeks who underwent clinically indicated abdominal/pelvic FTC CT examinations.[14] For each patient, the image data included, at a minimum, patient anatomy from the lower thorax to the pubic symphysis. Given that the patients represent a range of gestational ages, the fetus was not visible in 5 patients due the pregnancies being in the early stages. In these cases, either the uterus or the gestational sac was used as a surrogate organ for the fetus. For each patient, the uterus, gestational sac, and fetus were semi-automatically segmented from the axial images, depending on what was visible in the image data. The three-dimensional geometric centroid of the fetus was calculated based on the segmented boundaries. For each patient, an estimate of patient size in form D_w was determined from the image data per AAPM Report 220.[24] The patient size was determined as the D_w measured at the image containing the three-dimensional geometric centroid of the fetus.[14] If the fetus was not present, then D_w was estimated at the image containing three-dimensional geometric centroid of either the uterus or gestational sac.[14] DE_f is defined and was measured as the distance from the anterior skin surface to the most anterior part of the fetus.[14] DE_f was therefore measured at the slice containing the most anterior part of the fetus. Voxels containing the uterus were modeled as soft tissue, and the voxels of the gestational sac were modeled as water.[14] All voxels containing the fetus were modeled as either soft tissue or fetal bone depending on Hounsfield number.[14] The remaining voxels outside of the contoured regions were identified as a specific tissue type (lung, fat, water, muscle, bone, air) using a Hounsfield number lookup table.[26] **Table I** contains a list of the patient gestational ages and the organs of interest used in this study. **Figure 1** shows axial images of the centroid of the region of interest demonstrating the development of voxelized patient models for 3 of the pregnant patients.

II.B Monte Carlo Simulation Tool

A Monte Carlo software package, MCNPX (Monte Carlo N-Particle eXtended version 2.7.a), was utilized for all simulations.[27,28] The source code of MCNPX was modified to model MDCT scanner geometries and spectra.[29–32] The code is capable of selecting the appropriate energy spectrum data reflecting a range of scanner models previously generated using the "equivalent source" method by Turner et al.[33] and other user-specified variables such as scan length and helical pitch. All simulations were conducted in photon transport mode with a 1 keV low-energy cut-off. Additionally, all simulations were performed with 10^7 particle histories. All MC simulations were performed with the voxelized patient models at isocenter. In the case of TCM simulations, an additional text file with information on individual table location, tube angle, and tube current value throughout the scan was utilized in the simulation. Validation of this MC simulation package under a variety of conditions including TCM has been previously reported.[30,34–36]

II.C Modeling Tube Current Modulation (TCM) Scans

As actual TCM schemes are scanner make and model dependent, TCM modeling was limited to the specific scanner modeled previously by McMillan et al.[37] The method was used to estimate the TCM scheme from one manufacturer (CAREDose4D, Siemens Healthineers, Forchheim Germany). Therefore, only TCM scans using CAREDose4D[38] from the Definition AS64 were simulated. The methodology is summarized below in Section II.C.1. **Table II** contains the scanning protocol for TCM CT simulations. For each pregnant patient model, the TCM curves were estimated for an abdomen/pelvis scan. A $CTDI_{vol}$ value was then derived for each TCM curve based on the average mA across the scan.

II.C.1 Creation of TCM Functions

Using the methodology described in McMillan et al.,[37] TCM schemes were created for each of the pregnant patient models. As described therein, the TCM schemes generated are specific to one manufacturer's TCM algorithm. A brief summary of the methods described in McMillan et al.[37] are provided below.

II.C.1.1 Estimating Patient Size Using Attenuation Profiles

TCM typically adapts the tube current in response to the patient attenuation characteristics from the CT localizer radiograph. However, no localizer information is available for these patients. Therefore, a simulated CT radiograph was generated for each patient using MCNPX in order to acquire estimates of attenuation.

To generate the TCM schemes used in this investigation, the first step was to create a simulated abdominal/pelvic CT scan radiograph by simulating projections along the length of each patient's image data in 1 mm increments. When combined with a simulated in air scan, the result is the generation of patient attenuation profiles in the anterior-posterior (AP) direction. **Figure 2** depicts the methodology for generating the simulated CT radiograph. From these patient attenuation profiles, an estimate of the AP dimension of patient size was generated. This involved emulating methods employed by the manufacturer and included using a moving average filter on the attenuation profile and then determining the maximum attenuation from the profile.[39] The AP patient dimension was calculated at each table position using the maximum attenuation normalized by the linear attenuation coefficient of water at a given beam energy (assumed to be 120 kVp and having an equivalent energy of 60 keV).

The lateral (LAT) patient dimension was estimated using data derived from the simulated AP scan radiographs described above and applying a mathematical model that involves the elimination of outside air, the CT table and low-attenuation regions through the application of thresholds to the patient attenuation profile.[39,40] Additionally, in order to generate the LAT patient estimates from the AP estimates, the CAREDose4D estimation algorithm applies a table offset correction factor to account for the patient not being at isocenter in the image data. Once determined, these estimates of AP and LAT dimensions of patient size were used as the inputs to the methods to estimate Siemens TCM schemes described. AP and LAT patient dimension estimates were determined at each 1 mm step.

II.C.1.2 Estimating Tube Current Modulation Schemes from Attenuation Data

II.C.1.2.1 Estimating Longitudinal Tube Current Modulation

In the CAREDose4D AEC algorithm, tube current is first determined by comparing the actual patient attenuation from the CT radiograph to reference patient attenuation values hardcoded in the AEC alorgithm.[38,41] The AP and LAT water-equivalent estimates of patient size were determined from simulated CT radiographs in the previous section. The estimation of longitudinal modulation is based on the maximum attenuation at each table position from either the AP or LAT direction. Therefore, the maximum attenuation at each table position, i, $A_{max}(i)$ is determined by taking the maximum of the calculated AP and LAT size values for each tale position as shown in **Equation 1**:

$$A_{\max}(i) = \max\left(\exp\left(\mu_{water,kVp} \times AP(i)\right), \exp\left(\mu_{water,kVp} \times LAT(i)\right)\right) \quad (1)$$

where $\mu_{water,kVp}$ is the linear attenuation coefficient of water for a given beam energy. For this investigation, $\mu_{water,kVp}$ was set to 0.2 cm^{-1} for a 120 kVp beam.

After the maximum attenuation at each table position is calculated, tube current values (mA) at each table position, i, are calculated from the corresponding patient attenuation using **Equation 2**:

$$mA(i) = \frac{QRM \times pitch}{t} \times \left(\frac{A_{\max}(i)}{A_{ref}} \right)^{b} \quad (2)$$

where *QRM* is the quality reference effective tube current-time product (effective mAs) set on the scanner by the user,[41] *t* is the gantry rotation time, pitch is the user selected pitch value, $A_{max}(i)$ is the maximum patient attenuation at each table location *i*, A_{ref} is the protocol-specific reference attenuation value specified by the manufacturer,[41] and *b* is a strength parameter that can be set according to individual preferences for the tube current increase and decrease. The default strength setting for all Siemens CT scanners (including all scanners used in this investigation) is "Average" and corresponds to a *b* value of 0.33 for attenuation greater than A_{ref} and 0.5 for attenuation less than A_{ref}.[41,42] Applying **Equation 2** to the patient attenuation profiles determined at each table position from the simulated radiograph yielded an estimate of the maximum tube current at each table position and corresponds to the longitudinal modulation based upon attenuation characteristics.

II.C.1.2.2 Estimating Angular Tube Current Modulation

This AEC algorithm also modulates the tube current angularly according to angular attenuation measurements (i.e. angular or x-y modulation).[38] The only patient attenuation data used were the attenuation data derived from the simulated radiograph and was based on the AP and LAT attenuation profiles described above. Attenuation values between these ordinal positions of the tube gantry were obtained through interpolation to derive an estimate of the angular attenuation. In addition, a gantry rotation time-dependent parameter is utilized that limits the amount of modulation allowed at a given table position.[43]

II.C.1.2.3. Combining Longitudinal and Angular Modulation

Combining the longitudinal modulation scheme from Section II.C.1.2.1 and the angular modulation scheme from Section II.C.1.2.2 generated an estimated tube current profile. For the estimated tube current, the tube current at each table position, *i*, is based on the longitudinal modulation value multiplied by the angular modulation value.[37] For this work, the operating limits for tube current values were 665 mA for 120 kVp. (This was the limit for a Definition AS64, but that limit is higher for later scanners). An example TCM curve for one pregnant patient model is illustrated in **Figure 3**.

II.D Modeling Fixed Tube Current (FTC) Scans

For the FTC scans, four different 64 slice MDCT scanner models were used. These were (a) LightSpeed VCT (GE Medical Systems Waukesha, WI), (b) Brilliance 64, (Philips Medical Systems, Cleveland, OH), (c) Aquilion 64 (Toshiba Medical Systems, Inc., Otawara, Japan), and (d) Definition AS64 (Siemens Healthineers, Forchheim, Germany). For each scanner model, the equivalent source method[33] was used to determine the equivalent spectra and equivalent bowtie filtration profile. The nominal collimation, measured beam width, HVL, and $CTDI_{vol}$ per mAs for each scanner are described in **Table III**. The following technique was used for each scanner: 120 kVp, 400 mA, 0.5 s rotation time, and a pitch of 1. The beam collimation used was the widest available on each scanner model. For each scanner model, physical measurements were made using the 32 cm diameter CTDI phantom to determine the $CTDI_{vol}$ under these scan conditions (kVp, bowtie, etc.) and were reported on a mGy/mAs basis. $CTDI_{vol}$ values for each scanner were achieved by multiplying $CTDI_{vol}$ per values mAs by the tube current-rotation time product (effective mAs). These scanner models were incorporated into the MC simulation tools described in Section II.B.

II.E Fetal Dose Estimates

The nomenclature employed in this study was adapted from Turner et al.[21] Using voxelized models of patient anatomy described in Sections II.A, MC simulations of both TCM and FTC abdomen/pelvis CT examinations were performed to estimate the absolute dose to the fetus (D_{fetus}) for each pregnant patient model. For this study, D_{fetus} was taken as the ratio of total energy imparted to the total fetal mass.

Normalized fetal dose estimates, nD_{fetus}, were obtained by dividing D_{fetus} from the MC simulations by $CTDI_{vol}$. The differences of nD_{fetus} for TCM relative to FTC were compared for one scanner (Definition AS64). nD_{fetus} estimates were also used (1) to investigate an exponential relationship between nD_{fetus} and patient size in terms of D_w (Section II.E.1), (2) to explore a bivariate linear relationship between nD_{fetus} and both D_w and DE_f (Section II.E.2), and (3) to compare nD_{fetus} to the SSDE *f*-factors. Regression equations describing the correlations between nD_{fetus} with either D_w or both D_w and DE_f served as the means to generate scan technique-independent fetal dose estimates for any patient size. Additionally, for the FTC scans, $\overline{nD_{fetus}}$ was calculated by averaging the nD_{fetus} across the four scanners on a per patient basis and was used to investigate an exponential relationship with D_w, a bivariate relation with D_w and DE_f, and a comparison with SSDE *f*-factors. For FTC scans, the coefficient of variations (CoV) across the four scanners were also calculated on a per patient basis.

II.E.1 Fetal dose conversion coefficients as a function of D_w using an exponential model

The first approach is consistent with the observed exponential relationships between $CTDI_{vol}$-normalized organ dose and patient size demonstrated by Turner et al.[22] and used in AAPM report 204.[23] This exponential relationship between nD_{fetus} and D_w is defined in **Equation 3**:

$$nD_{fetus,1}(D_w)=A_0 \times exp(-B_0 \times D_w) \quad (3)$$

where $nD_{fetus,1}(D_w)$ represents fetal dose conversion coefficients as a function of D_w using the exponential model and A_0 and B_0 are exponential regression coefficients. A_0 and B_0 were determined

by performing the regression of nD_{fetus} and D_w across all patient models and were determined separately for TCM and FTC scans. For FTC scans, nD_{fetus} for the FTC scans from each manufacturer and $\overline{nD_{fetus}}$ were correlated separately using **Equation 3**. $\overline{nD_{fetus,1}}(D_w)$ was used to represent the exponential model using $\overline{nD_{fetus}}$. In order to gauge the strength of these correlations, the coefficient of determination (R^2) was used.

II.E.2 Fetal dose conversion coefficients as a function of D_w and DE_f using a bivariate linear model

The second approach is based on Angel et al.[14] wherein the relationship between nD_{fetus} and both D_w and DE_f is defined in **Equation 4**:

$$nD_{fetus,2}(D_w,DE_f)=A_1-B_1D_w-C_1DE_f \quad (4)$$

where $nD_{fetus,2}(D_w,DE_f)$ represents fetal dose conversion coefficients as a function of D_w and DE_f using the bivariate linear model, and A_1, B_1, and C_1 are regression coefficients. A_1, B_1, and C_1 were determined by performing the regression of nD_{fetus} with D_w and DE_f across all patient models and were determined separately for TCM and FTC scans. The bivariate linear regression was performed using GraphPad Prism 6.00 for Mac OS X (GraphPad Software, La Jolla, California, USA, www.graphpad.com). A user-defined regression model was configured for the analysis of two independent variables. This regression analysis was performed using the FTC scans from each manufacturer and $\overline{nD_{fetus}}$. $\overline{nD_{fetus,2}}(D_w,DE_f)$ was used to represent the bivariate linear model using $\overline{nD_{fetus}}$. As in Section II.E.1, the coefficient of determination (R^2) was used to gauge the strength of the correlation.

II.E.3 Comparison of nD_{fetus} to SSDE f-factors

The nD_{fetus} estimates from TCM and FTC were compared to the SSDE *f*-factors based on the 32 cm $CTDI_{vol}$ phantom from AAPM Report 204 using the *f*-factors as a reference. **Equation 5**, taken from AAPM Report 204 (Equation A-1 of the report), was used to generated the conversion factors across the patient sizes investigated in this study and is as follows:

$$SSDE\ f\text{-}factors = A_0 \times exp(-B_0 \times D_w) \quad (5)$$

where A_0 = 3.70 and B_0 = 0.037.[23] $\overline{nD_{fetus}}$ estimates were also compared to the SSDE *f*-factors. The differences relative to SSDE *f*-factors were expressed in terms of percentage (%) for each patient. In addition, for the exponential model regression analyses performed in Section II.E.1, the SSDE *f*-factors were included as a point of reference with shaded regions corresponding to ± 20% and ± 25% of the SSDE *f*-factors.

III. RESULTS

III.A TCM comparison to FTC for a single scanner

Table IV contains the D_w estimates, DE_f, $CTDI_{vol}$ estimates for TCM scans, absolute fetal dose (D_{fetus}) values for AS64 TCM simulations and AS64 FTC simulations, normalized fetal dose (nD_{fetus}) values for AS64 TCM simulations and AS64 FTC simulations, and differences of TCM nD_{fetus} relative to FTC nD_{fetus}. D_w estimates ranged from 25.3 cm to 35.6 cm. DE_f estimates ranged from 3.4 cm to 10.9 cm. The $CTDI_{vol}$ for TCM ranged from 6.9 mGy to 17.3 mGy. The $CTDI_{vol}$ for FTC for the AS64 was 15.6 mGy across all patients. For TCM, nD_{fetus} differences relative to FTC ranged from -5% to 23%, with a mean of 6% across all patients.

III.B Fetal dose conversion coefficients as a function of D_w using an exponential model

III.B.1 TCM and FTC exponential relationships for a single scanner

Figure 4 shows the exponential model regression analysis for both TCM and FTC simulations for the AS64 nD_{fetus} data tabulated in **Table IV**. The R^2 values of the TCM and FTC was observed to be 0.73 and 0.70, respectively. The results of the regression analysis are tabulated in **Table V**.

III.B.2 FTC exponential relationships for four scanners

For the FTC scan protocol described in Section II.E, the $CTDI_{vol}$ for the LightSpeed VCT, Brilliance 64, and Aquilion 64 scanners was 17.7 mGy, 12.5 mGy, and 24.6 mGy, respectively, across all patients. As mentioned in Section III.A, the $CTDI_{vol}$ for FTC for the AS64 was 15.6 mGy across all patients. The nD_{fetus} for each of the four scanners in FTC mode and $\overline{nD_{fetus}}$ are tabulated in **Table VI**. The CoV ranged from 10% to 14%. The mean CoV across all patients was 12%. **Figure 5** contains the FTC regression analyses for the four scanners. The R^2 values for the exponential model for the LightSpeed VCT, Brilliance 64, and Aquilion 64 in FTC mode were observed to be 0.63, 0.60, and 0.64, respectively. From Section III.B.1, the R^2 value of the AS64 in FTC mode was observed to be 0.70. The exponential regression coefficients and coefficients of determination for FTC fetal dose estimates from the four scanners are shown in **Table VII**. **Figure 6** shows regression analysis of $\overline{nD_{fetus,1}}(D_w)$, which yielded an R^2 of 0.64.

III.C *Fetal dose conversion coefficients as a function of D_w and DE_f using a bivariate linear model*

Table VIII contains the results for the multivariate regression analyses for the all the scanners used in this investigation. The multivariate regression using the bivariate linear model for nD_{fetus} from TCM was observed to have an R^2 value of 0.78. The R^2 values for $nD_{fetus,2}(D_w,DE_f)$ for the LightSpeed VCT, Brilliance 64, Aquilion 64, and AS64 in FTC mode were observed to be 0.74, 0.76, 0.75, and 0.77, respectively. The R^2 value of $\overline{nD_{fetus,2}}\left(D_w,DE_f\right)$ was observed to be 0.75.

III.D Comparisons to SSDE *f*-factors

III.D.1 SSDE f-factor comparison to TCM and FTC nD_{fetus} from a single scanner

Comparison of the AS64 TCM and FTC nD_{fetus} to SSDE are tabulated in **Table IX**. **Figure 7** shows the same exponential model regression analyses shown in **Figure 4** with the addition of the SSDE *f*-factors as a point of reference. Shaded areas corresponding to ± 20% and ± 25% of the SSDE *f*-factors were also added. For TCM (n=24), 15 patients in this study had nD_{fetus} within ± 20% of the SSDE *f*-factors, and 21 patients had nD_{fetus} within ± 25% of the SSDE *f*-factors. For FTC (n=24), 20 patients in this study had nD_{fetus} within ± 20% of the SSDE *f*-factors, and 22 patients had nD_{fetus} within ± 25% of the SSDE *f*-factors. When considering both TCM and FTC scans (n=48), 35 instances of nD_{fetus} were within ± 20% of the SSDE *f*-factors, and 43 instances of nD_{fetus} were within ± 25% of the *f*-factors. **Table X** contains a summary of the relation of nD_{fetus} to the SSDE *f*-factors per **Figure 7**.

III.D.2 SSDE f-factor comparison to $\overline{nD_{fetus}}$

Table XI contains the comparisons $\overline{nD_{fetus}}$ to the SSDE *f*-factors on a per patient basis. The differences with respect to the SSDE *f*-factors ranged from -29% to 17%. A mean difference of 0% was observed between $\overline{nD_{fetus}}$ and the SSDE *f*-factors. **Figure 8** shows the regression analyses for the four scanners shown in **Figure 5** with the addition of the SSDE *f*-factors as a point of reference.

Shaded areas corresponding to ± 20% and ± 25% of the SSDE *f*-factors were also added to **Figure 8**. All but two patients had $\overline{nD_{fetus}}$ that were within the ± 20% tolerance specified by AAPM Report 204. **Figure 9** shows $\overline{nD_{fetus,1}}(D_w)$ with the addition of the SSDE *f*-factors as a point of reference and shaded regions corresponding to ± 20% and ± 25% of the SSDE *f*-factors.

IV. DISCUSSION

In this work, MC simulation methods were applied to 24 pregnant patient models (originally developed by Angel et al.[14]) in order to estimate fetal dose from CT abdomen/pelvis exams using TCM and FTC. TCM was applied to one scanner model for which TCM schemes could be estimated. Additionally, this scanner model and three additional scanner models were used to estimate fetal dose from FTC scans. For both TCM and FTC scans, the resulting fetal doses were normalized by scanner output ($CTDI_{vol}$) and parameterized with respect to water equivalent diameter (D_w) to create size-specific, scan technique-independent fetal dose estimates. A bivariate linear model was also investigated correlating normalized fetal dose with D_w and a metric of fetal position in terms of fetal depth (DE_f). The resulting fetal dose coefficients were then compared to the SSDE conversion coefficients (the SSDE *f*-factors from AAPM Report 204).

As described in Section II.A, D_w was measured at the image containing the three-dimensional geometric centroid of the fetus or surrogate organ (being uterus and gestational sac), the same location used by Angel et al.[14] The image data for these patients were not originally reconstructed at the maximum available field of view (FOV). Because of this, nearly all of the patients (n=22) had small portions of peripheral anatomy outside of the FOV. Since the voxelized models were based upon the image data, the calculated D_w from the simulated topogram underestimates D_w for these cases. This underestimation of AP and LAT dimensions from anatomy outside of the FOV also affects the inputs necessary to estimate TCM schemes. Underestimated patient size yields lower tube current values. The decreased tube current values would also yield decreased $CTDI_{vol}$ estimates from the average tube current across the entire scan range. However, the voxelized model itself will also be affected as there

will be less tissue to attenuate the photons in the simulations. Therefore, the net effect of a slightly underestimated patient size due to small portions of peripheral anatomy outside the FOV on nD_{fetus} should have minimal impact to the study results.

When comparing TCM to FTC (performed for the Definition AS64 in this study), the coefficients of determination of 0.73 and 0.70, for $nD_{fetus,1}(D_w)$ for both TCM and FTC, respectively, suggest that D_w explains much of the variation of nD_{fetus}. $nD_{fetus,2}(D_w,DE_f)$ using both D_w and DE_f for TCM yielded a coefficient of determination of 0.78. This finding suggests that a knowledge of D_w and DE_f may give a better estimate for fetal dose than D_w alone. As can be noted in **Figure 4** and in **Table IV**, the TCM conversion coefficients are systematically greater than the FTC conversion coefficients by roughly 6% on average. The increase in fetal dose from TCM relative to FTC is most probably due to AEC response to pelvic anatomy. The fetal extent included the pelvis for most of the patients, as is shown in **Figure 3**. As such, the fetus experienced an elevated tube current due to the attenuation of the pelvis. However, TCM was only simulated for one TCM technology, so it is not clear whether this 6% would be observable for all TCM technologies. Further study would therefore be needed to ascertain if this difference exists with other AEC systems.

For the Definition AS64, TCM conversion coefficients of the fetus and surrogate organs (when the fetus was not present) were observed to be greater than the SSDE conversion coefficients by 17%, as can be seen from **Figure 7** and **Table IX**. The higher conversion coefficients would imply a higher absolute fetal dose relative to SSDE for a given $CTDI_{vol}$. One potential reason for the conversion coefficients being higher than the SSDE *f*-factors is that the *f*-factors were based on the average absorbed dose to organs located in the abdomen using MC simulations of FTC abdomen protocols for voxelized phantom models.[21–23] The soft-tissue organs within are effectively water-equivalent in composition, in contrast to fetal anatomy, which is comprised both of water equivalent soft-tissue voxels and bone voxels. The mass energy-absorption coefficients of bone to water is greater than unity, meaning the absorbed dose to the fetus should be higher than absorbed dose to any of the abdominal organs,[20] so for a given $CTDI_{vol}$, the nD_{fetus} should be greater than the normalized dose to abdominal organs. On the other hand, the surrogate organs, the uterus and gestational sac (5 of

the 24 patients), also experienced normalized doses higher than SSDE conversion coefficients. These two organs are, as described in Section II.B, comprised of soft-tissue and water, respectively, unlike fetal anatomy. Therefore, what these results suggests is that the variance from the SSDE *f*-factors may be scanner-specific. This conclusion is additionally supported by the variability observed for nD_{fetus} for FTC simulations of the other scanners in Section III.B.[21] These imply variance from the SSDE *f*-factors can be related to properties of the scanner itself, such as the scanner x-ray source.

However, for the Definition AS64, the majority of patients in this study, for both TCM and FTC, had nD_{fetus} within ± 20% of the SSDE *f*-factors and within ± 25% of the SSDE *f*-factors, as **Table X** shows. SSDE was never intended to be applied to fetal dose estimates. However, AAPM Report 204 stipulates a 10-20% tolerance of estimated patient dose from size-specific, scan technique-independent conversion factors and actual patient dose.[23] Though there were some patients that had differences from the SSDE *f*-factors greater that 20%, results from this study indicate that normalized doses from both TCM and FTC are mostly within this tolerance range. This suggests that, within the patient size range used in this study, the SSDE *f*-factors can provide a reasonable (within ± 25%) estimate of normalized fetal dose estimates for both TCM and FTC abdominal/pelvis scans.

Additionally, this study also investigated nD_{fetus} for FTC averaged across the four different scanner manufacturers ($\overline{nD_{fetus}}$). In the case of $\overline{nD_{fetus,1}}(D_w)$, the coefficient of determination was observed to be 0.64 with respect to D_w, meaning D_w explains roughly two thirds of the variation seen in $\overline{nD_{fetus}}$. The regression analyses using the exponential model performed for each scanner shown in **Figure 5** highlight the observed variability of normalized dose across scanners as discussed above,[21] albeit within 15%. $\overline{nD_{fetus,2}}(D_w,DE_f)$ yielded a coefficient of determination of 0.75. Only two patients (ID1 and ID4), both of which are early-term patients, had $\overline{nD_{fetus}}$ beyond the tolerance specified in AAPM Report 204. One possible explanation for this observation is that, for these two patients, the DE_f was larger relative (10.6 cm and 10.9 cm, respectively) to the other patients. As can be seen in **Figure 10**, the larger DE_f implies that the organs of interest for these two patients are positioned deeper within the

pelvis as compared with two other early-term patients (ID5 and ID3) and are thus provided with more inherent shielding, which decreased their normalized dose. Given this variation in fetal position in early-term patients, the inclusion of DE_f in the bivariate model may explain the improvement of correlative ability over the exponential model.

Across patients, the mean $\overline{nD_{fetus}}$ difference from the SSDE *f*-factors was observed to be 0.4%. Furthermore, the curves representing $\overline{nD_{fetus,1}}(D_w)$ and the SSDE *f*-factors are fairly similar within the patient size range of this study, as can be seen in **Figure 9**. These points further buttress the conclusion made above, namely, that within the patient size range used in this study, for FTC scans, the SSDE *f*-factors can provide a reasonable estimate of nD_{fetus}. This result is intuitive given that AAPM Report 204 was concerned with estimating the dose to the central region of abdomen CT exams using FTC and derived the $CTDI_{vol}$ conversion coefficients by incorporating normalized dose values across multiple scanner manufacturers.[23] However, this being said, for early-term patients, the position of the uterus or gestational sac can vary due a variety of factors, as highlighted in **Figure 10**. Therefore, a wider tolerance from SSDE may be necessary to account for the variability of early-term maternal anatomy.

V. CONCLUSION

Results from this study suggest that fetal dose from both TCM and FTC CT scans of pregnant patients of various gestational ages and patient sizes may be reasonably estimated using models that incorporate (1) scanner-reported $CTDI_{vol}$ and (2) with D_w as a metric for patient size metric to account for patient size variation. Moreover, more accurate estimates of fetal dose can be obtained with knowledge of DE_f if it is available. The results from this study also imply that the SSDE *f*-factors can provide a reasonable (within ± 25%) estimate of normalized fetal dose across scanners for the range of patient sizes investigated herein.

There are still a few important limitations worth mentioning. The first is that, as detailed in Section II.E, the TCM data for the patients in this study were based off the attenuation characteristics from a simulated CT localizer and estimates from one manufacturer's AEC algorithm. Ideally, patient D_w information and TCM data directly from the scanner would be available. However, since they were not available for these patients, estimates of patient D_w from simulations were generated. Moreover, estimating the AEC algorithm of other manufacturers is beyond the scope of this work. The second limitation is that, as mentioned above, the variability of early-term maternal anatomy can have an effect on the ability of SSDE to serve as a surrogate for fetal dose. This study, however, only considered five early-term patients. The data in this study suggest a detailed investigation of fetal dose in early-term pregnant patients is warranted and hence will be the subject of future work. A third limitation is that only scans of the abdomen/pelvis region were considered. Head and chest scans of the patients were not considered for this study as the pregnant patient models used in this study did not include this anatomy. To extend this work to scans of other anatomic regions, whole-body patient models of maternal anatomy would be needed such as the RPI pregnant patient models.[44] However, fetal dose contributions from head or chest scans are expected to be negligible.[45,46] Lastly, the available image resolution was not sufficient to investigate dose to specific fetal organs such as the thyroid and red bone marrow. This study averaged the dose across the entire fetal volume and thus included the dose to individual developing organs into a single estimate of fetal dose. Extending this work could therefore also include investigating dose to developing fetal organs, provided that the resolution of fetal anatomy is sufficient enough to make this a possibility.

ACKNOWLEDGEMENTS

This work was supported in part by a grant the NIH (T32-EB002101). M.M.G's department has a master research agreement with Siemens Healthcare. E.A. is an employee of Canon Medical Systems, USA.

REFERENCES

1. ICRP. The 2007 Recommendations of the International Commission on Radiological Protection. *ICRP Publ 103 Ann ICRP 37*. 2007.

2. ICRP 70. Basic Anatomical & Physiological Data for use in Radiological Protection - The Skeleton. *Ann ICRP*. 1995;(2). doi:10.1016/S0146-6453(00)80004-4.

3. Cristy M. Active bone marrow distribution as a function of age in humans. *Phys Med Biol*. 1981;26:389-400. doi:10.1088/0031-9155/26/3/003.

4. Felmlee JP, Gray JE, Leetzow ML, Price JC. Estimated fetal radiation dose from multislice CT studies. *Am J Roentgenol*. 1990;154(1):185-190. doi:10.2214/ajr.154.1.2104708.

5. Hurwitz LM, Yoshizumi T, Reiman RE, et al. Radiation dose to the fetus from body MDCT during early gestation. *Am J Roentgenol*. 2006;186(3):871-876. doi:10.2214/AJR.04.1915.

6. Shrimpton PC, Jones DG. Normalised Organ Doses for X Ray Computed Tomography Calculated Using Monte Carlo Techniques and a Mathematical Anthropomorphic Phantom. *Radiat Prot Dosim*. 1993;49(1-3):241-243.

7. Stamm G, Nagel HD. [CT-expo--a novel program for dose evaluation in CT]. *Rofo*. 2002;174(12):1570-1576. doi:10.1055/s-2002-35937.

8. Huda W, Ogden KM, Lavallee RL, Roskopf ML, Scalzetti EM. In-patient to isocenter KERMA ratios in CT. *Med Phys*. 2011;38(10):5362. doi:10.1118/1.3635222.

9. Huda W, Randazzo W, Tipnis S, Frey DG, Mah E. Embryo Dose Estimates in Body CT. *Am J Roentgenol*. 2010;194(4):874-880. doi:10.2214/AJR.09.4032.

10. Damilakis J, Tzedakis A, Perisinakis K, Papadakis AE. A method of estimating conceptus doses

resulting from multidetector CT examinations during all stages of gestation. *Med Phys*. 2010;37(12):6411-6420. doi:10.1118/1.3517187.

11. Gilet AG, Dunkin JM, Fernandez TJ, Button TM, Budorick NE. Fetal Radiation Dose During Gestation Estimated on an Anthropomorphic Phantom for Three Generations of CT Scanners. *Am J Roentgenol*. 2011;196(5):1133-1137. doi:10.2214/AJR.10.4497.

12. Damilakis J, Perisinakis K, Voloudaki a, Gourtsoyiannis N. Estimation of fetal radiation dose from computed tomography scanning in late pregnancy: depth-dose data from routine examinations. *Invest Radiol*. 2000;35(9):527-533. doi:10.1097/00004424-200009000-00002.

13. Jaffe T a., Yoshizumi TT, Toncheva GI, Nguyen G, Hurwitz LM, Nelson RC. Early first-trimester fetal radiation dose estimation in 16-MDCT without and with automated tube current modulation. *Am J Roentgenol*. 2008;190(4):860-864. doi:10.2214/AJR.07.2925.

14. Angel E, Wellnitz C V, Goodsitt MM, et al. Radiation dose to the fetus for pregnant patients undergoing multidetector CT imaging: Monte Carlo simulations estimating fetal dose for a range of gestational age and patient size. *Radiology*. 2008;249(1):220-227. doi:10.1148/radiol.2491071665.

15. Maynard MR, Geyer JW, Aris JP, Shifrin RY, Bolch W. The UF family of hybrid phantoms of the developing human fetus for computational radiation dosimetry. *Phys Med Biol*. 2011;56(15):4839-4879. doi:10.1118/1.3611623.

16. Maynard MR, Long NS, Moawad NS, et al. The UF Family of hybrid phantoms of the pregnant female for computational radiation dosimetry. *Phys Med Biol*. 2014;59(15):4325-4343. doi:10.1088/0031-9155/59/15/4325.

17. Gu J, Bednarz B, Caracappa PF, Xu XG. The development, validation and application of a multi-detector CT (MDCT) scanner model for assessing organ doses to the pregnant patient

and the fetus using Monte Carlo simulations. *Phys Med Biol*. 2009;54(9):2699-2717. doi:10.1088/0031-9155/54/9/007.

18. Xu XG, Taranenko V, Zhang J, Shi C. A boundary-representation method for designing whole-body radiation dosimetry models: pregnant females at the ends of three gestational periods--RPI-P3, -P6 and -P9. *Phys Med Biol*. 2007;52(23):7023-7044. doi:10.1088/0031-9155/52/23/017.

19. Gu J, Xu XG, Caracappa PF, Liu B. Fetal doses to pregnant patients from CT with tube current modulation calculated using Monte Carlo simulations and realistic phantoms. *Radiat Prot Dosimetry*. 2013;155(1):64-72. doi:10.1093/rpd/ncs312.

20. Kelaranta A, Kaasalainen T, Seuri R, Toroi P, Kortesniemi M. Fetal radiation dose in computed tomography. *Radiat Prot Dosimetry*. 2015;165(1-4):226-230. doi:10.1093/rpd/ncv097.

21. Turner AC, Zankl M, DeMarco JJ, et al. The feasibility of a scanner-independent technique to estimate organ dose from MDCT scans: using CTDIvol to account for differences between scanners. *Med Phys*. 2010;37(4):1816-1825.

22. Turner AC, Zhang D, Khatonabadi M, et al. The feasibility of patient size-corrected, scanner-independent organ dose estimates for abdominal CT exams. *Med Phys*. 2011;38(2):820-829. doi:10.1118/1.3533897.

23. AAPM Task Group 204. *Size-Specific Dose Estimates (SSDE) in Pediatric and Adult Body CT Examinations*. College Park, MD; 2011.

24. AAPM Task Group 220. *Use of Water Equivalent Diameter for Calculating Patient Size and Size-Specific Dose Estimates (SSDE) in CT*. College Park, MD; 2014.

25. Zhang D, Savandi AS, Demarco JJ, et al. Variability of surface and center position radiation dose in MDCT: Monte Carlo simulations using CTDI and anthropomorphic phantoms. *Med*

Phys. 2009;36(3):1025-1038. doi:10.1118/1.3078053.

26. Demarco JJ, Solberg TD, Smathers JB. A CT-based Monte Carlo simulation tool for dosimetry planning and analysis. *Med Phys*. 1998;25:1-11.

27. Pelowitz DB. *MCNPX User's Manual Version 2.7.0, Los Alamos National Laboratory Report LA-CP-11-00438 (LANL, Los Alamos, NM, 2011).*; 2011.

28. AAPM (American Association of Physicists in Medicine). *Monte Carlo Reference Data Sets for Imaging Research: The Report of AAPM Task Group 195*.; 2015.

29. Jarry G, DeMarco JJ, Beifuss U, Cagnon CH, McNitt-Gray MF. A Monte Carlo-based method to estimate radiation dose from spiral CT: from phantom testing to patient specific models. *Phys Med Biol*. 2003;48(16):2645-2663. http://www.ncbi.nlm.nih.gov/pubmed/12974580.

30. DeMarco JJ, Cagnon CH, Cody DD, et al. A Monte Carlo based method to estimate radiation dose from multidetector CT (MDCT): cylindrical and anthropomorphic phantoms. *Phys Med Biol*. 2005;50(17):3989-4004. doi:10.1088/0031-9155/50/17/005.

31. DeMarco JJ, Cagnon CH, Cody DD, et al. Estimating radiation doses from multidetector CT using Monte Carlo simulations: effects of different size voxelized patient models on magnitudes of organ and effective dose. *Phys Med Biol*. 2007;52(9):2583-2597. doi:10.1088/0031-9155/52/9/017.

32. Gatsonis CA, Aberle DR, Berg CD, et al. The national lung screening trial: Overview and study design. *Radiology*. 2011;258(1). doi:10.1148/radiol.10091808.

33. Turner AC, Zhang D, Kim HJ, et al. A method to generate equivalent energy spectra and filtration models based on measurement for multidetector CT Monte Carlo dosimetry simulations. *Med Phys*. 2009;36(6). doi:10.1118/1.3117683.

34. Bostani M, Mueller JW, McMillan K, et al. Accuracy of Monte Carlo simulations compared to

in-vivo MDCT dosimetry. *Med Phys*. 2015;42(2). doi:10.1118/1.4906178.

35. Bostani M, McMillan K, Demarco JJ, Cagnon CH, McNitt-Gray MF. Validation of a Monte Carlo model used for simulating tube current modulation in computed tomography over a wide range of phantom conditions/challenges. *Med Phys*. 2014;41(11). doi:10.1118/1.4887807.

36. Khatonabadi M, Zhang D, Mathieu K, et al. A comparison of methods to estimate organ doses in CT when utilizing approximations to the tube current modulation function. *Med Phys*. 2012;39(8):5212-5228. doi:10.1118/1.4736807.

37. McMillan K, Bostani M, Cagnon CH, et al. Estimating Patient Dose from CT Exams That Use Automatic Exposure Control: Development and Validation of Methods to Accurately Estimate Tube Current Values. *Med Phys*. May 2017. doi:10.1002/mp.12314.

38. Flohr T. *CARE Dose4D White Paper*.; 2011.

39. Wolf, H, Suss, C, Popescu S. US Patent No. 20050058249 A1, U.S. Patent and Trademark Office. 2005.

40. Raupach,R, Schaller,A, Suss, C WH. US Patent No. 7289595 B2, U.S. Patent and Trademark Office. 2007.

41. Favazza CP, Yu L, Leng S, Kofler JM MC. Automatic Exposure Control Systems Designed to Maintain Constant Image Noise: Effects on Computed Tomography Dose and Noise Relative to Clinically Accepted Technique Charts. *J Comput Assist Tomogr*. 2015;39(3):437-442. doi:10.1097/RCT.0000000000000221.

42. Mahesh M. *MDCT Physics : The Basics: Technology, Image Quality and Radiation Dose*. Philadelphia: Lippincott, Williams and Wilkins; 2009.

43. Popescu, S, Hentschel, D, Strauss, K, Wolf H. US Patent No. 5867555 A, U.S. Patent and Trademark Office. 1999.

44. Xu XG, Taranenko V, Zhang J, Shi C. A boundary-representation method for designing whole-body radiation dosimetry models: Pregnant females at the ends of three gestational periods - RPI-P3, -P6 and -P9. *Phys Med Biol*. 2007;52(23):7023-7044. doi:10.1088/0031-9155/52/23/017.

45. Woussen S, Vanbeckevoort D, Bosmans H. Clinical indications and radiation doses to the conceptus associated with CT imaging in pregnancy : a retrospective study. 2016:979-985. doi:10.1007/s00330-015-3924-8.

46. Goldberg-Stein SA, Liu B, Hahn PF, Lee SI. Radiation Dose Management: Part 2, Estimating Fetal Radiation Risk From CT During Pregnancy. *Am J Roentgenol*. 2012;198(4):W352-W356. doi:10.2214/AJR.11.7458.

Figure 1: Images in the first row, from left to right, represent early, mid-term, and late-term pregnant patients. Images in the second row show the uterus (yellow), gestational sac (green), and fetus (red) segmented from the images of these pregnant patients. Adapted with permission from Figure 3 of Angel et al.[14]

Figure 2: A) Voxelized representation of patient model (sagittal view) and **B)** simulated CT radiograph (AP view). The simulated CT radiograph was generated by simulating projections at 1 mm increments along the length of the voxelized patient model and dividing the resulting projections by a reference air scan. The legend below **A)** is color-coded for the material designations for each voxel.

Figure 3: Estimated TCM scheme for a pregnant patient who received a clinically indicated CT examination. The TCM scheme is overlaid on an image of the simulated CT localizer radiograph (AP orientation) of the pregnant patient. The portion of the scan range in which the fetus is located is indicated with yellow dashed lines.

Figure 4: $nD_{fetus,1}(D_w)$ for the TCM and FTC scans from the AS64. $nD_{fetus,1}(D_w)$ represents the exponential model using nD_{fetus} and D_w for TCM and FTC scans.

Figure 5: The results here are only for FTC scans. $nD_{fetus,1}(D_w)$ for the **A)** LightSpeed VCT, **B)** Brilliance 64, **C)** Aquilion 64, and **D)** AS64. The $CTDI_{vol}$ values for the four scanners were 17.7 mGy

for the LightSpeed VCT, 12.5 mGy for the Brilliance, 24.6 mGy for the Aquilion, and 15.6 mGy for the AS64. $nD_{fetus,1}(D_w)$ represents the exponential model using nD_{fetus} and D_w for each of the four scanners.

Figure 6: Regression analysis for $\overline{nD_{fetus,1}}(D_w)$ using the exponential model. $\overline{nD_{fetus,1}}(D_w)$ represents the exponential model using $\overline{nD_{fetus}}$ and D_w.

Figure 7: The same regression analyses shown in **Figure 4** accompanied by the SSDE *f*-factors from AAPM Report 204 as a point of reference and shaded areas corresponding to ± 20% and ± 25% of the SSDE *f*-factors. A summary of the doses that fall within ± 20% and ± 25% of the SSDE *f*-factors are tabulated in **Table X**.

Figure 8: $nD_{fetus,1}(D_w)$ for the **A)** LightSpeed VCT, **B)** Brilliance 64, **C)** Aquilion 64, and **D)** Definition AS64 shown in **Figure 5** with the SSDE *f*-factors from AAPM Report 204 included as a point of reference. In addition, shaded areas corresponding to ± 20% and ± 25% of the SSDE *f*-factors are also shown.

Figure 9: $\overline{nD_{fetus,1}}(D_w)$ accompanied with the SSDE *f*-factors and the shaded regions corresponding to ± 20% and ± 25% of the SSDE *f*-factors for comparison.

Figure 10: Axial and sagittal images showing the variability of early-term maternal anatomy. For ID1 in **A)** and ID4 in **B)**, the greater DE_f means that the uterus (yellow) and gestational sac (green), respectively, are situated deeper within the pelvis and hence provided the fetus more shielding. For ID5 in **C)**, the uterus and gestation sac extend anteriorly and for ID3 in **D)**, a distended bladder (outlined in cyan) pushes uterus more anteriorly.

Table I: Gestational age and region of interest used for all subjects

ID	Gestational Age (weeks)	Region of Interest
1	< 5	Uterus
2	5.0	Ges. Sac
3	5.0	Ges. Sac
4	6.6	Ges. Sac
5	7.1	Ges. Sac
6	12.1	Fetus
7	14.3	Fetus
8	14.9	Fetus
9	17.0	Fetus
10	17.1	Fetus
11	18.5	Fetus
12	20.3	Fetus
13	22.0	Fetus
14	23.7	Fetus
15	24.0	Fetus
16	24.4	Fetus
17	25.0	Fetus
18	27.0	Fetus
19	27.4	Fetus
20	27.4	Fetus
21	28.3	Fetus
22	29.4	Fetus
23	35.0	Fetus
24	35.9	Fetus

Table II: Scanning parameters used for the TCM scan on Siemens Definition AS64 using CAREDose4D

Parameter	Setting
kVp	120
Quality reference mAs (QRM)	200
Rotation time (s)	0.5
Pitch	1.0
Nominal collimation (mm)	19.2 (64 × 0.6 FFS)
Measured collimation (mm)	23.8
Bowtie filter	Body
HVL (mm Al)	8.2
$CTDI_{vol}$ (mGy/mAs)	0.078

Table III: Scanners used for fixed tube current (FTC) scans and associated parameters. The nominal collimation, measured beam width, HVL, and CTDI per mAs for the Definition AS64 listed in **Table II** of Section II.C are presented here for comparison.

Manufacturer	Model	Nominal collimation (mm)	Measured beam width (mm)	HVL (mm Al)	$CTDI_{vol}$ (mGy/mAs)
GE	LightSpeed VCT	40 (64 × 0.625)	42.4	7.8	0.089
Philips	Brilliance 64	40 (64 × 0.625)	43.7	8.6	0.062
Toshiba	Aquilion 64	32 (64 × 0.5)	36.9	5.5	0.123
Siemens	Definition AS64	19.2 (64 × 0.6 FFS)	23.8	8.2	0.078

Table IV: For all patients listed in **Table I**, this table includes patient size metric (D_w), fetal depth (DE_f), patient $CTDI_{vol}$ estimates for TCM scans, D_{fetus} from TCM and FTC, nD_{fetus} from TCM and FTC, as well as TCM nD_{fetus} difference (%) relative to FTC. The $CTDI_{vol}$ for FTC for was 15.6 mGy.

ID	D_w (cm)	DE_f (cm)	TCM $CTDI_{vol}$ (mGy)	Absolute fetal dose, D_{fetus} (mGy)		Normalize fetal dose (nD_{fetus})		nD_{fetus} Difference (%)
				TCM	FTC	TCM	FTC	
1	33.5	10.6	15.4	18.2	14.9	1.18	0.96	23
2	25.6	4.2	8.7	14.6	23.3	1.68	1.50	12
3	28.9	7.6	6.9	10.9	25.6	1.57	1.64	-5
4	29.2	10.9	11.8	14.1	16.6	1.20	1.07	12
5	27.3	5.9	9.2	17.3	25.0	1.87	1.61	16
6	25.3	4.6	9.1	16.2	28.1	1.77	1.81	-2
7	32.0	6.5	12.7	17.8	21.2	1.40	1.37	3
8	28.0	7.1	10.1	14.5	21.7	1.43	1.40	2
9	29.6	7.7	11.2	16.5	22.3	1.47	1.43	3
10	25.9	6.7	9.1	15.0	24.3	1.65	1.56	6
11	26.6	5.6	9.5	17.3	27.6	1.83	1.77	3
12	34.6	8	13.4	15.3	16.8	1.14	1.08	6
13	30.6	4.7	15.9	22.4	21.5	1.41	1.38	2
14	35.6	6.3	15.6	17.0	15.9	1.09	1.02	7
15	29.7	5.6	8.9	13.3	22.3	1.50	1.44	5
16	28.2	6.6	9.5	14.0	22.5	1.47	1.45	1
17	27.9	2.5	12.7	19.8	23.8	1.56	1.53	2
18	27.9	9	8.0	11.6	22.5	1.45	1.45	1
19	30.8	3.6	11.7	17.9	23.1	1.52	1.48	3
20	35.6	6	17.3	20.2	16.8	1.17	1.08	8
21	34.0	5.5	13.6	17.5	18.6	1.29	1.20	8
22	31.7	3.5	16.7	21.8	18.9	1.30	1.22	7
23	28.5	5.1	11.5	15.5	20.5	1.36	1.32	3
24	35.3	3.4	16.1	20.1	17.4	1.24	1.12	11
							Mean	6

Table V: $nD_{fetus,1}(D_w)$ and R^2 values for the AS64 TCM and FTC scans.

Normalized Dose	A_0	B_0	R^2
AS64 TCM	4.68	0.040	0.73
AS64 FTC	5.28	0.045	0.70

Table VI: The results below are only for FTC scans. nD_{fetus} for the four scanners, $\overline{nD_{fetus}}$, and CoV across the four scanners. The FTC nD_{fetus} for the AS64 was included for comparison. CoV results reflect the variation among the four scanner models on a per patient basis.

ID	nD_{fetus}				$\overline{nD_{fetus}}$	CoV (%)
	LightSpeed VCT	Brilliance 64	Aquilion 64	AS64		
1	0.89	0.68	0.85	0.96	0.84	14
2	1.36	1.11	1.36	1.50	1.33	12
3	1.54	1.20	1.51	1.64	1.47	13
4	0.98	0.75	0.93	1.07	0.93	14
5	1.52	1.27	1.55	1.61	1.48	10
6	1.73	1.42	1.74	1.81	1.67	10
7	1.30	1.03	1.25	1.37	1.24	12
8	1.32	1.03	1.29	1.40	1.26	13
9	1.35	1.07	1.34	1.43	1.30	12
10	1.48	1.15	1.45	1.56	1.41	13
11	1.71	1.37	1.68	1.77	1.64	11
12	1.02	0.79	0.98	1.08	0.97	13
13	1.34	1.09	1.32	1.38	1.28	10
14	0.97	0.76	0.92	1.02	0.92	12
15	1.38	1.08	1.33	1.44	1.31	12
16	1.38	1.09	1.34	1.45	1.32	12
17	1.49	1.21	1.45	1.53	1.42	10
18	1.38	1.07	1.33	1.45	1.31	12
19	1.45	1.18	1.41	1.48	1.38	10
20	1.04	0.81	0.99	1.08	0.98	12
21	1.16	0.90	1.11	1.20	1.09	12
22	1.19	0.95	1.13	1.22	1.12	11
23	1.27	1.00	1.22	1.32	1.20	12
24	1.10	0.88	1.05	1.12	1.04	10
				Mean	1.25	12

Table VII: $nD_{fetus,1}(D_w)$ and R^2 for the four scanners, along with $\overline{nD_{fetus,1}}(D_w)$ and its R^2 values. The AS64 FTC $nD_{fetus,1}(D_w)$ regression coefficients are shown here for comparison.

Conversion Coefficients	A_0	B_0	R^2
LightSpeed VCT FTC	4.78	0.044	0.63
Brilliance 64 FTC	4.09	0.046	0.60
Aquilion 64 FTC	5.21	0.047	0.64
AS64 FTC	5.28	0.045	0.70
$\overline{nD_{fetus,1}}(D_w)$	4.82	0.046	0.64

Table VIII: $nD_{fetus,2}(D_w,DE_f)$ regression coefficients and R^2 values for the bivariate linear models. $\overline{nD_{fetus,2}}(D_w,DE_f)$ regression coefficients are also included.

Conversion Coefficients	A_1	B_1	C_1	R^2
AS64 TCM	3.26	0.055	0.026	0.78
LightSpeed VCT FTC	3.13	0.053	0.036	0.74
Brilliance 64 FTC	2.61	0.045	0.036	0.76
Aquilion 64 FTC	3.22	0.057	0.037	0.75
AS64 FTC	3.32	0.059	0.030	0.77
$\overline{nD_{fetus,2}}(D_w,DE_f)$	3.07	0.053	0.035	0.75

Table IX: Comparison of the AS64 TCM and FTC nD_{fetus} to the SSDE *f*-factors

ID	AS64 TCM nD_{fetus}	AS64 FTC nD_{fetus}	SSDE *f*-factors	Difference from the SSDE *f*-factors (%)	
				AS64 TCM	AS64 FTC
1	1.18	0.96	1.08	9	-12
2	1.68	1.50	1.45	16	3
3	1.57	1.64	1.28	22	28
4	1.20	1.07	1.31	-9	-16
5	1.87	1.61	1.36	38	19
6	1.77	1.81	1.46	21	24
7	1.40	1.37	1.14	22	19
8	1.43	1.40	1.33	8	5
9	1.47	1.43	1.25	18	15
10	1.65	1.56	1.43	16	9
11	1.83	1.77	1.40	31	27
12	1.14	1.08	1.04	10	4
13	1.41	1.38	1.20	17	15
14	1.09	1.02	1.00	9	2
15	1.50	1.44	1.25	21	15
16	1.47	1.45	1.32	11	10
17	1.56	1.53	1.33	17	15
18	1.45	1.45	1.33	9	9
19	1.52	1.48	1.19	27	22
20	1.17	1.08	1.00	16	7
21	1.29	1.20	1.06	21	13
22	1.30	1.22	1.16	12	5
23	1.36	1.32	1.30	4	1
24	1.24	1.12	1.01	23	11
			Mean	17	10

Table X: Summary table of nD_{fetus} points within the bounds of ± 20% and ± 25% of the SSDE *f*-factors

	TCM (n=24)	FTC (n=24)	TCM + FTC (n=48)
nD_{fetus} within ± 20%	15 (62.5%)	20 (83.3%)	35 (72.9%)
nD_{fetus} within ± 25%	21 (87.5%)	22 (91.7%)	43 (89.6%)
nD_{fetus} beyond ± 25%	3 (12.5%)	2 (8.3%)	5 (10.4%)

Table XI: Comparison of $\overline{nD_{fetus}}$ to the SSDE *f*-factors

ID	$\overline{nD_{fetus}}$	SSDE *f*-factors	Difference from the SSDE *f*-factors (%)
1	0.84	1.08	-22
2	1.33	1.45	-8
3	1.47	1.28	15
4	0.93	1.31	-29
5	1.48	1.36	9
6	1.67	1.46	15
7	1.24	1.14	8
8	1.26	1.33	-5
9	1.30	1.25	4
10	1.41	1.43	-1
11	1.64	1.40	17
12	0.97	1.04	-7
13	1.28	1.20	7
14	0.92	1.00	-8
15	1.31	1.25	5
16	1.32	1.32	0
17	1.42	1.33	7
18	1.31	1.33	-2
19	1.38	1.19	16
20	0.98	1.00	-2
21	1.09	1.06	2
22	1.12	1.16	-3
23	1.20	1.30	-8
24	1.04	1.01	2
		Mean	0.4